Direct characterization of nanocrystal size distribution using Raman spectroscopy

AIP | Journal of Applied Physics

Direct characterization of nanocrystal size distribution using Raman spectroscopy

İlker Doğan and Mauritius C. M. van de Sanden

Citation: J. Appl. Phys. **114**, 134310 (2013); doi: 10.1063/1.4824178
View online: http://dx.doi.org/10.1063/1.4824178
View Table of Contents: http://jap.aip.org/resource/1/JAPIAU/v114/i13
Published by the AIP Publishing LLC.

JOURNAL OF APPLIED PHYSICS **114**, 134310 (2013)

Direct characterization of nanocrystal size distribution using Raman spectroscopy

İlker Doğan[1,a)] and Mauritius C. M. van de Sanden[1,2,b)]
[1]*Department of Applied Physics, Eindhoven University of Technology, P.O. Box 513, 5600MB Eindhoven, The Netherlands*
[2]*Dutch Institute for Fundamental Energy Research (DIFFER), P.O. Box 1207, 3430BE Nieuwegein, The Netherland*

(Received 29 July 2013; accepted 17 September 2013; published online 4 October 2013)

We report a rigorous analytical approach based on one-particle phonon confinement model to realize direct detection of nanocrystal size distribution and volume fraction by using Raman spectroscopy. For the analysis, we first project the analytical confinement model onto a generic distribution function, and then use this as a fitting function to extract the required parameters from the Raman spectra, i.e., mean size and skewness, to plot the nanocrystal size distribution. Size distributions for silicon nanocrystals are determined by using the analytical confinement model agree well with the one-particle phonon confinement model, and with the results obtained from electron microscopy and photoluminescence spectroscopy. The approach we propose is generally applicable to all nanocrystal systems, which exhibit size-dependent shifts in the Raman spectrum as a result of phonon confinement. © *2013 AIP Publishing LLC*. [http://dx.doi.org/10.1063/1.4824178]

I. INTRODUCTION

Size dependent opto-electronic properties present in semiconductor nanocrystals makes them prospective materials for applications like Li-ion batteries,[1] charge storing devices,[2] light emitting diodes,[3] solar cells,[4] and spectrum converters to absorb and manipulate the high energy region of the solar spectrum by means of carrier multiplication.[5–7]

The effective control of the nanocrystal size distribution is critical as the size dependency is a determinant parameter on device performance and efficiency. For instance, the efficiency of a silicon nanocrystal (Si-NC) based tandem solar cell[8] can reach a maximum value if the size distribution in each nanocrystal layer is monodisperse. As the Si-NCs in each of these layers have a well-defined band-gap (as a result of monodisperse size distribution), size variations result in inefficient absorption of photons deteriorating the device efficiency and performance. A control on the size and size distribution could be realized in an optimized synthesis environment that involves the synthesis of nanocrystals and analysis of the size distribution.

The lack of a fast, simple and reliable analysis technique on the size distribution of nanocrystals precludes fulfilling the requirements of an optimized synthesis-analysis route. A versatile analysis technique on the size distribution is essential for research on controlled synthesis of Si-NCs, and would be practical in the study of other types of semiconductor nanocrystal systems. The techniques reported in the literature for the analysis of the average size and the size distribution of Si-NCs are X-ray diffraction (XRD),[9,10] transmission electron microscopy (TEM),[10] photoluminescence spectroscopy (PL),[11] and Raman spectroscopy (RS).[12,13] XRD provides information on the material morphology, but data acquisition is time consuming. In addition, XRD only provides information on the volume average size of nanocrystals from the broadening of the diffraction peak,[9] due to the lack of sensitivity to the individual sizes in a distribution—separate analysis of sizes is unfeasible in a multimodal distribution. TEM affords analysis of multimodal size distributions and material morphology. The downside of this analysis method is the sample preparation procedure that is time consuming. In addition, size distribution analysis is a challenge on densely packed nanocrystal ensembles due to the insufficient image resolution on individual nanocrystals. PL provides information on the particle size distribution from the size dependent visible luminescence of Si-NCs.[11] However, not all the Si-NCs can be analyzed with PL as this diagnostic tool requires nanocrystals with sufficient optical properties (that makes sure the luminescence is from Si-NCs, instead of defects).[14] In addition, large nanocrystals, which are out of the confinement regime, cannot be probed with PL as they have indirect band structure, which hampers the rate of radiative recombination. The limitations of these analysis tools raise the need for a diagnostic tool that can determine the size distribution in a reliable, simple, and time efficient way.

Raman spectroscopy (RS) is a well-established technique to analyze the morphology and size distribution of Si-NCs. When compared with TEM, RS is a time efficient technique in the sense that sample preparation is unnecessary. A major advantage of RS is that the different phases of the analyzed material are observed by their characteristic lattice vibration modes or phonons.[12,15] Bulk crystalline silicon (c-Si) has a Lorentzian-shaped transverse optical phonon (TO) mode at 521 cm^{-1} and amorphous silicon (a-Si:H) has a broad phonon mode at 480 cm^{-1}.[16] In a finite size crystalline grain, the translational symmetry of the crystal lattice is no longer conserved due to the presence of grain boundaries that results in confinement of phonons. This leads to a red-shift and broadening of the bulk phonon mode of

[a)]Electronic mail: i.dogan@tue.nl
[b)]Electronic mail: m.c.m.vandesanden@differ.nl

crystalline silicon to lower wavenumbers with decreasing size—especially for sizes smaller than 20 nm.[12,17,18] Thus, unlike XRD, Raman spectrum is influenced by the presence of each silicon nanocrystal in a size distribution: the result is a red-shifted and broadened spectrum that relates to the nanocrystal size distribution. As a vibrational spectroscopy, RS allows the analysis of large Si-NCs out of the confinement regime and small nanocrystals with insufficient optical properties. This property is indeed an advantage over PL and facilitates the estimation of the volume fraction between small and large Si-NCs.[16,19]

In the literature, a number of models are developed to describe influence of nanocrystal size on the broadening and shift of the phonon peak.[12,20,21] Two models to describe the nanocrystal size according to the shift of the phonon peak are the bond polarizability model (BPM),[21] and the modified one-phonon confinement model (PCM).[12] BPM describes the polarizability of a nanocrystal system calculated by the sum of the contributions of each bond for a particular size. PCM describes the Raman spectrum of a nanocrystal, as a function of its crystal momentum, phonon frequency, phonon dispersion, and the degree of confinement. The degree of the phonon confinement (the smaller the size, the stronger the confinement) influences the width and position of the phonon peak. As these parameters are size-dependent, an equivalent representation of the PCM that depends only on the nanocrystal size can be derived. We can exploit this expression derived for a single nanocrystal to determine the size distribution parameters (mean size and skewness) by projecting the PCM onto a size distribution function.[17,22]

In this work, on the basis of the PCM, we will develop an analytical approach that is expressed in terms of nanocrystal size only, which will be used as a fitting function to directly determine the silicon nanocrystal size distribution. By using the analytical PCM model developed, we will show that volume fraction of nanocrystals with different sizes could be determined if a mixture of different size distributions are involved. We use the benchmark results on nanocrystal sizes obtained from TEM and PL, and compare them with RS results. We will also correlate sizes with PCM and BPM. Finally, we will discuss and summarize the advantages and limitations of our approach on extreme cases (monodisperse distributions, and extremely small Si-NCs), and the applicability of the method to other nanocrystal systems.

II. THEORY

The Raman effect is the inelastic scattering of light by lattice vibrations, which is observed when these vibrations change polarization–so that the change in the polarizability tensor with respect to the normal vibration co-ordinate is non-zero.[15] The active phonon in the Raman scattering process of bulk materials is in the center of the first Brillouin Zone (BZ) with $\boldsymbol{q} \sim 0$, where $\boldsymbol{q}$ is the crystal momentum. Classical electromagnetic radiation theory predicts Lorentzian-shaped Raman peaks from an oscillating dipole[15]

$$I(\omega, \boldsymbol{q}) = I_0 \int_{(\mathrm{BZ})} L(\omega, \boldsymbol{q}) d^3\boldsymbol{q}, \tag{1}$$

$$L(\omega, \boldsymbol{q}) = \frac{1}{\pi} \frac{\Gamma/2}{[\omega - \omega(\boldsymbol{q})]^2 + [\Gamma/2]^2}. \tag{2}$$

The Lorentzian $L(\omega,\boldsymbol{q})$ is a function of wavenumber ω (in units of cm^{-1}), phonon dispersion relation $\omega(\boldsymbol{q})$, and the characteristic full width at half maximum (FWHM) Γ of the Raman peak. For a silicon crystal, an empirical phonon dispersion relation is given by[18,23,24]

$$\omega(\boldsymbol{q}) = \omega_{Si}\left(1 - 0.23\left(\frac{q a_{\mathrm{Si}}}{2\pi}\right)^2\right), \tag{3}$$

where $\omega_{\mathrm{Si}} = 521\,\mathrm{cm}^{-1}$ is the optical phonon peak position, and $a_{\mathrm{Si}} = 0.543$ nm is the lattice constant of bulk crystalline silicon (and the FWHM of the optical phonon peak of bulk crystalline silicon is $\Gamma = \Gamma_{\mathrm{Si}} = 3\,\mathrm{cm}^{-1}$).[12,13,25]

Equation (1) represents the Raman spectrum for semi-infinite crystals—systems under long range translational symmetry. In a finite-size crystal, the translational symmetry of the lattice is no longer conserved due to the presence of grain boundaries that results in confinement of phonons, and triggers a red-shift (to the lower wavenumbers) of the characteristic phonon mode with decreasing size. The red-shift of the Raman spectrum with decreasing nanocrystal size is explained by the phonon confinement model (PCM),[12] where the infinite phonon wave function is projected on the first BZ of a finite-sized nanocrystal by a suitable weighting function $\psi(k_n,r)$ (Here, we use a sinc function.[12] A variety of other weighting functions leading to different degrees of confinements are also reported.[20,26–28] However, these confinement functions are arbitrarily chosen and lack a physical basis):

$$\psi(k_n, r) = \begin{cases} \sum_n \dfrac{\sin(k_n r)}{k_n r}, & r \le D/2 \\ 0, & r > D/2, \end{cases} \tag{4}$$

$\psi(k_n,r)$ is valid within the nanocrystal and vanishes at the boundary ($k_n = n\pi/D$, $n = 2,4,6,\ldots, n_{\max} < 2D/a_{\mathrm{Si}}$). With this form of $\psi(k_n,r)$, the phonon wave function in a nanocrystal is represented as a weighted superposition of sinusoidal waves, which describes the vibration of an atomic chain of length D. This ensures that the single phonon wave vector is strongest at the center of the nanocrystal and decays rapidly zero at the nanocrystal surface.[12] We employ the Fourier transform of the weighting function to switch from $\boldsymbol{k}$-space to $\boldsymbol{q}$-space so that the Fourier coefficients $C_n(\boldsymbol{q},D)$ are used to account for the size effects in the Raman spectrum[12]

$$C_n(\boldsymbol{q}, D) = 3\frac{\sin(qD/2)}{\pi^3 D^3 q({k_n}^2 - q^2)}. \tag{5}$$

Therefore, we define the single particle Raman spectrum of a spherical nanocrystal as

$$I(\omega, D, \boldsymbol{q}) \propto \rho[\omega] \int_{q_{\min}}^{q_{\max}} |C(\boldsymbol{q}, D)|^2 L(\omega, \boldsymbol{q}) 4\pi q^2 d\boldsymbol{q}, \tag{6}$$

where $\rho[\omega]$ is the Raman scattering efficiency,[29] which depends on the occupation distribution factor

$$\rho[\omega] \sim \frac{n(\omega)+1}{\omega} = \frac{\left(\exp(h\omega/kT)-1\right)^{-1}+1}{\omega}. \quad (7)$$

In Eq. (6), q is limited to in the range $[(n\pi - 1)/D, (n\pi + 1)/D]$ due to the momentum conservation.[12] Raman intensity of a nanocrystal can be approximately determined by considering the first component of the weighting function ($n=2$), as the other components strongly decay in intensity.[30] We remove the size dependency of the integral boundaries with a change of variables, i.e., $\mathcal{Q}=qD$. Thus, the Raman intensity of a single particle reads as

$$I(\omega,D) \propto \rho[\omega]\frac{1}{\pi D^3} \times \int_{2\pi-1}^{2\pi+1} \frac{4\pi\mathcal{Q}^2\left|3\frac{\sin(\mathcal{Q}/2)}{\pi^3\mathcal{Q}(4\pi^2-\mathcal{Q}^2)}\right|^2(\Gamma/2)}{\left[\omega-521\left(1-0.23\left(\frac{\mathcal{Q}a_{Si}}{2\pi D}\right)^2\right)\right]^2+(\Gamma/2)^2}d\mathcal{Q}. \quad (8)$$

Figure 1 shows the results of the integral in Eq. (8) for various Si-NC sizes. PCM leads to peak shifts when the nanocrystal size is smaller than 20 nm. In other words, silicon nanocrystals with sizes larger than 20 nm resemble bulk-like behavior.

Equation (8) enables the experimental analysis of single particles and particles with a monodisperse distribution. If a size distribution is involved, Eq. (8) needs to be projected onto a distribution function that is integrated over the size range in the following way:

$$I(\omega) = \int_{D_{min}}^{D_{max}} \Phi(D)\ I(\omega,D)dD, \quad (9)$$

where $\Phi(D)$ is a general unknown particle size distribution function. In principle, one can set the integral boundary as $[0,\infty]$.

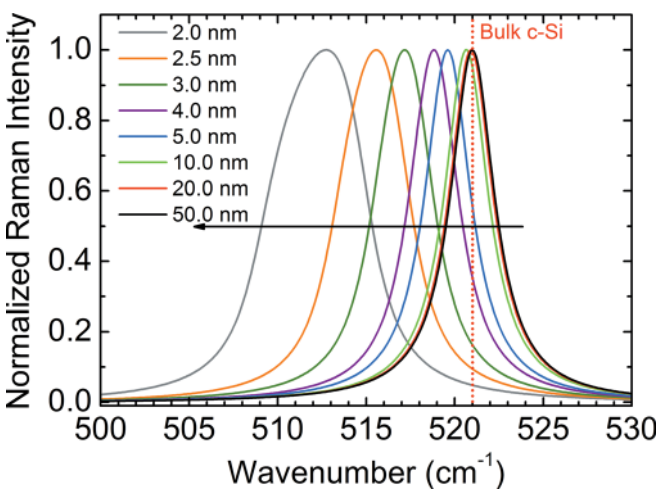

FIG. 1. Calculated Raman spectra of silicon nanocrystals with various sizes by employing the phonon confinement model (PCM) used in Eq. (8).

One should use Eq. (9) and fit to the experimental data to extract the parameters that will define the distribution function—the mean size D_0, and the width parameter, or skewness σ—to determine the nanocrystal size distribution. Before that, one should also evaluate the single particle PCM $I(\omega,D)$, to project it onto a generic size distribution function. The challenge here is that the average peak shift, peak broadening, and peak intensity depend on the nanocrystal size D through a complicated expression (Eq. (8)). In fact, we can re-define this expression in such a way it contains the size dependency in an explicit manner. As we know from the electromagnetic radiation theory, optical phonon mode of bulk silicon has a symmetric generalized Lorentzian peak shape.[15] For silicon nanocrystals, this symmetric shape of the Lorentzian function is conserved for the sizes down to 3.0 nm and an increased asymmetry is observed as the sizes get smaller (see Fig. 1). Our strategy here is to show that in a Raman spectrum of silicon nanocrystals with a size distribution, the one particle Raman spectra can be expressed as symmetric Lorentzian functions for sizes as small as 2.0 nm. In this way, it is possible to demonstrate an analytical and non-integral expression of the one particle PCM by means of a Lorentzian function for nanocrystals, where the particular parameters, i.e., peak intensity, peak broadening, and peak position, are expressed as functions of silicon nanocrystal size. We define the generalized Lorentzian $\mathcal{L}_{Si}(\omega,D)$ for silicon nanocrystals as follows:

$$\mathcal{L}_{Si}(\omega,D) = \frac{A(D)}{\pi}\frac{\Gamma_{NC}(D)/2}{[\omega-\omega_{NC}(D)]^2+[\Gamma_{NC}(D)/2]^2}. \quad (10)$$

Equation (10) contains explicit expressions for the intensity $A(D)$, peak broadening $\Gamma_{NC}(D)$, and peak position $\omega_{NC}(D)$, which could be expressed in terms of nanocrystal size by means of fitting Eq. (8) with Eq. (10) for various sizes (The fitting replicates the original model well, i.e., the coefficient of determination is $R^2>0.99$ for sizes down to 3.0 nm, $R^2>0.98$ for 2.5 nm and $R^2>0.96$ for 2.0 nm. The coefficient of determination decreases as a result of increased asymmetry at smaller sizes). The determined values for the peak intensity, average broadening, and average shift as a function of silicon nanocrystal size are demonstrated in Fig. 2. The parameters of $\mathcal{L}_{Si}(\omega,D)$ resemble a linear behavior when plotted on a double logarithm plot. We observe a deviation from the linearity in the peak intensity and average broadening for Si-NCs smaller than 3.0 nm. This deviation may result in misinterpretation of the actual particle size (for sizes smaller than 3.0 nm) in the case of a monodisperse distribution. However, as we will show (in Fig. 3), if a size distribution is involved, the Raman spectrum could be replicated as long as the smallest sizes occupy the tail of the distribution. We determine the size dependent parameters from Fig. 2, which will be used for replicating the one particle Raman spectrum, as follows:

$$\begin{aligned} A(D) &= 1.4\times10^{-2}D^{-3}, \\ \Gamma_{NC}(D) &= \Gamma_{Si}+60.0D^{-4}, \\ \omega_{NC}(D) &= \omega_{Si}-34.8D^{-2}. \end{aligned} \quad (11)$$

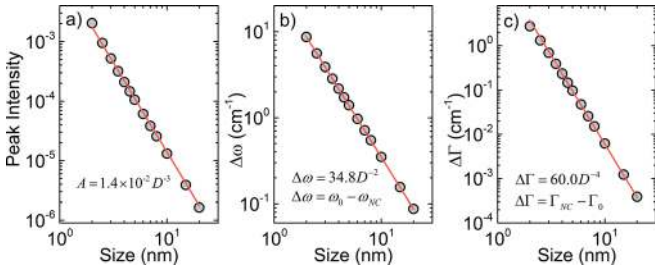

FIG. 2. (a) Peak intensity, (b) average shift, (c) and the average broadening of silicon nanocrystals as a function of size. Data points are obtained by fitting Eq. (8) with Eq. (10) for different sizes from 2.0 to 20.0 nm. The exponents on the particle sizes are set as fixed.

In Eq. (11), the exponents on the particle sizes are set as fixed. For large or semi-infinite silicon nanocrystals, which are outside of the phonon confinement regime, $\Gamma_{NC}(D) \sim \Gamma_{Si}$ and $\omega_{NC}(D) \sim \omega_{Si}$, and Eq. (10) converges to the Lorentzian shape of bulk silicon.

According to Eq. (11), the intensity of the phonon peak of individual silicon nanocrystals is roughly proportional to the D^{-3}, where D is the nanocrystal size. On the other hand, the absolute scattering efficiency depends on the density of phonons, which scales with the interaction volume, or D^3 for spherical nanocrystals. Therefore, the Raman scattering intensity of a silicon nanocrystal is independent of the nanocrystal size, but is dependent on the number of nanocrystals with that size. The size distribution of nanocrystals can be determined by setting the intensity term independent of nanocrystal size, i.e., dropping the intensity term to unity in Eq. (10). Therefore, we can correlate the intensity of phonon frequencies of different sizes with their relative number of nanocrystals in a size distribution. Now using the exact expressions in Eq. (11) for $\mathcal{L}_{Si}(\omega,D)$, we can determine the size distribution of silicon nanocrystals in the confinement regime by fitting the experimental Raman spectrum using the following relation:

$$I(\omega) = \int_{D_{min}}^{D_{max}} \Phi(D)\mathcal{L}_{Si}(\omega, D)dD. \qquad (12)$$

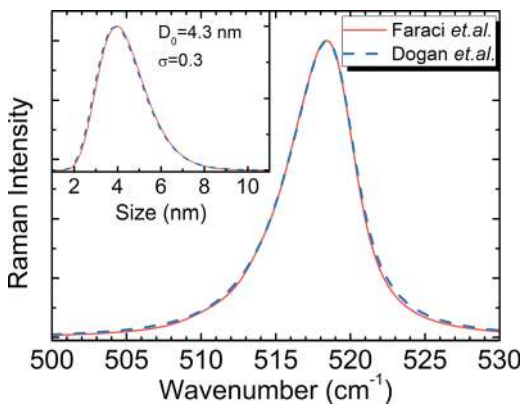

FIG. 3. Calculated Raman spectrum of silicon nanocrystals by using the PCM and analytical form of the PCM. Solid line: Raman intensity calculated from Eq. (9) in which $I(\omega,D)$ is defined by Faraci *et al.*[12] Dashed line: Raman intensity calculated from Eq. (12) in which $\mathcal{L}_{Si}(\omega,D)$ is defined in this work. Inset shows the corresponding size distributions.

Equation (12) explicitly contains size dependent terms, and analytical non-integral form of the one particle PCM can be projected onto the particle size distribution function. As a demonstration, we compare the calculated Raman spectra of silicon nanocrystals with a size distribution by using the PCM (Eq. (9)) and the analytical PCM (Eq. (12)). We use a lognormal function to represent the nanocrystal size distribution

$$\Phi(D) = \frac{1}{\sigma D\sqrt{2\pi}} \exp\left\{-\frac{\log[D/D_0]^2}{2\sigma^2}\right\}. \qquad (13)$$

In Eq. (13), D_0 is the mean size and σ is the width parameter for shape profile, i.e., skewness of the distribution.

Figure 3 demonstrates the calculated Raman spectra of silicon nanocrystals with a lognormal size distribution. For the similar shape of the Raman peak, the mean size of the distribution is determined as 4.25 nm from PCM used by Faraci *et al.*[12] and as 4.30 nm from our analytical PCM. The width parameters are determined as the same, i.e., $\sigma = 0.3$. Inset of Fig. 3 shows the size distribution of Si-NCs determined from the two models. From these size distributions, we prove that analytical PCM replicates the PCM[12] well when a size distribution is involved. The slight difference in mean sizes is due to the deviation of the one particle analytical PCM for sizes smaller than 3.0 nm.

III. EXPERIMENT

Free standing spherical silicon nanocrystals (Si-NCs) with a bimodal size distribution are synthesized in an argon/-silane gas mixture by using a remote expanding thermal plasma deposition technique (ETP).[31] During synthesis, an argon flow of 20 sccs, and a varying silane flow from 1 to 10 sccs are used with a total gas pressure of 1 mbar. Synthesized material is collected on copper substrates. Raman spectroscopy (RS) measurements are performed with a Renishaw Raman microscope equipped with a 514 nm laser, a grating with 1800 lines/mm, and a CCD detector, and with a measurement step size of 1.7 cm^{-1}. The laser power during measurements is fixed at 0.3 W/mm^2. This laser power is sufficiently lower than the threshold power (1 $mW/\mu m^2$) for the Fano effect,[32,33] which is an artificial broadening and red-shift as a result of laser induced heating. It is also experimentally verified that the selected laser power does not induce any artificial shift and broadening in the Raman spectrum of Si-NCs. XRD is performed by a diffractometer using Cu K_α radiation. The (111) diffraction peak of crystalline silicon is analyzed for the morphology of Si-NCs. Transmission electron microscope (TEM) images are obtained after transferring the deposited nanocrystals to holey carbon films. Statistical analyses are performed on the TEM images to estimate the size distribution of Si-NCs. Photoluminescence spectroscopy (PL) is used to analyze the optical emission from the size distribution of Si-NCs. Samples are illuminated using a 334 nm continuous wave Ar laser. Luminescence is detected with a UV-grade fiber, connected to a spectrometer, which is coupled to a nitrogen cooled CCD. Size distribution of silicon nanocrystals is

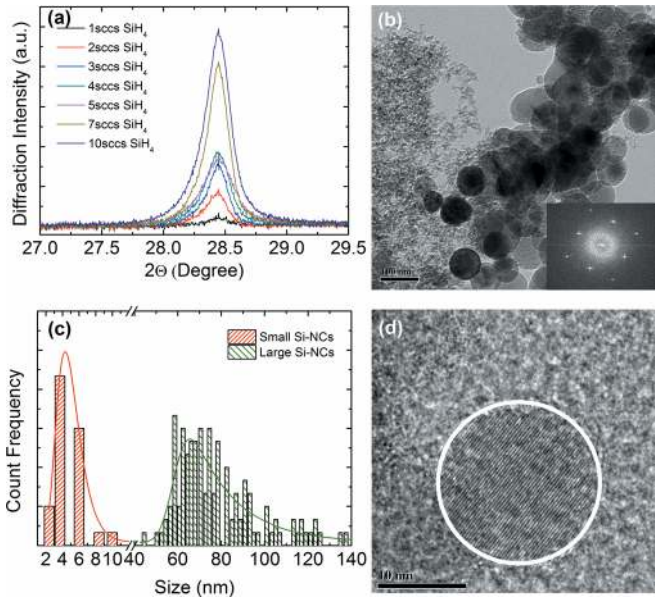

FIG. 4. (a) Si (111) diffraction peaks observed from XRD as a function of silane flow rate. (b) TEM images of Si-NCs synthesized with 4 sccs SiH_4 flow. Inset of (b) shows the fast Fourier transform (FFT) image from large Si-NCs. (c) Statistical size distribution data that reveals the presence of bimodal size distribution acquired from TEM images. (d) HRTEM of a small Si-NC with spherical and monocrystalline morphology.

obtained by correlating their optical emission with their size dependent band-gap energies using the empirical formula shown in the work of Delerue *et al.*[34]

IV. RESULTS AND DISCUSSION

We start with discussing the effect of stress on free standing Si-NCs. Stress on silicon nanocrystals induces a peak shift in the Raman spectrum and the absolute size dependent shift can only be determined by eliminating the stress-related shift. The origin of the stress is reported as[35] the lattice mismatch between the silicon nanostructure and the host matrix. Figure 4(a) demonstrates the characteristic (111) XRD diffraction peak of crystalline silicon centered at $2\theta = 28.4°$. Observed (111) peaks of Si-NCs at $2\theta = 28.4°$ indicate that small and large Si-NCs are under minimal, if not no strain as 28.4° is the Si (111) peak in unstrained polycrystalline Si.[9] Stress-free nature of Si-NCs synthesized in gas phase reactions are by virtue of their free standing morphology.[31] Therefore, we rule out stress-related shifts in the analysis of Raman spectrum of free standing Si-NCs. Increase of the XRD intensity is a sign of increase of the amount of deposited material on the substrates. Size analysis of nanocrystals using XRD is possible[36] —a volume-averaged size value can be determined. Employing XRD could work in monodisperse size distributions or in size distributions with a single mode to find the average size. If a multimodal size distribution is involved, using XRD provides unreliable results[31] due to the lack of sensitivity on modes of the distributions.

Figures 4(b) and 4(d) show the TEM images of Si-NCs synthesized using a silane flow rate of 4 sccs. TEM images reveal the presence of small and large Si-NCs in the deposits (Fig. 4(b)) as reported previously.[31] Fast Fourier transform (FFT) (inset of Fig. 4(b)) and high resolution images (Fig. 4(d)) conclude the spherical shape and monocrystalline morphology of small and large Si-NCs. Statistical size analysis (Fig. 4(c)) demonstrates a bimodal size distribution: small Si-NCs are in the size range 2–10 nm (with a peak size of about 4–5 nm), and large Si-NCs are in the size range 50–120 nm (with a peak size of about 70 nm). In addition, both distributions have lognormal shape—an expected observation considering the method in which nanocrystals are synthesized under the influence of diffusion and convection forces in well-defined residence times.[31] We observe the bimodal size distribution of Si-NCs with lognormal distribution profiles from all samples. We will use this feature while analyzing the measured Raman spectra in detail.

Figure 5 demonstrates measured Raman spectra for various silane flow rates. As observed from Fig. 5, the analyzed Si-NCs are predominantly crystalline (Additional support: inset of Fig. 7 in Ref. 31). The peak position of the Raman spectra red-shifts with silane flow rate and indicates a decrease in the average Si-NC size.[31] In addition, we observe a peak broadening with increased silane flow. These broad peaks are asymmetric and demonstrate dissimilar behavior than the Raman spectra in Fig. 1. For individual or monodisperse Si-NCs, both the low and high wavenumber (LW and HW, respectively, demonstrated in Fig. 5) parts of the full width at half maximum (FWHM) shift with decreasing nanocrystal size according to the PCM (Fig. 1).[12] However, in Fig. 5, the position of the LW red-shifts while the position of the HW remains almost unchanged for silane flow rates from 2 to 10 sccs. This finding states that the distribution of Si-NCs is not monodisperse—smaller Si-NCs are involved while large Si-NCs are still present in the deposits with increased flow rates of silane. Therefore, the experimental Raman spectra should be deconvoluted to determine the contributions from small and large Si-NCs.

To estimate the size distribution of small Si-NCs, we use the following strategy: First, we use the unshifted Lorentzian (the one-particle analytical PCM) to represent large silicon nanocrystals ($D \gtrsim 20$ nm), which is the semi-infinite size approximation of Eq. (10); with $\Gamma_{NC} = \Gamma_{Si} = 3\,cm^{-1}$ and $\omega_{NC} = \omega_{Si} = 521\,cm^{-1}$. As large

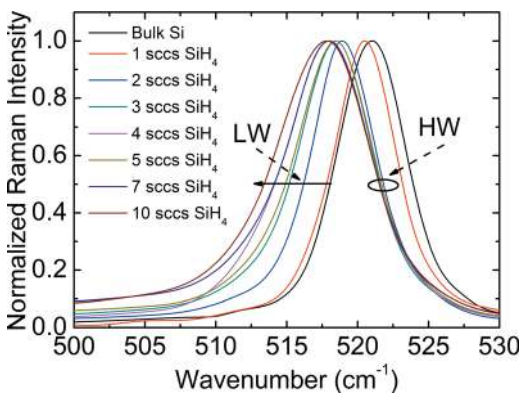

FIG. 5. Normalized Raman spectra of free standing Si-NCs for various silane flow rates. The asymmetry, broadening, and the shift of the Raman peak increase with silane flow. Raman spectrum of the bulk c-Si is also shown for comparison.

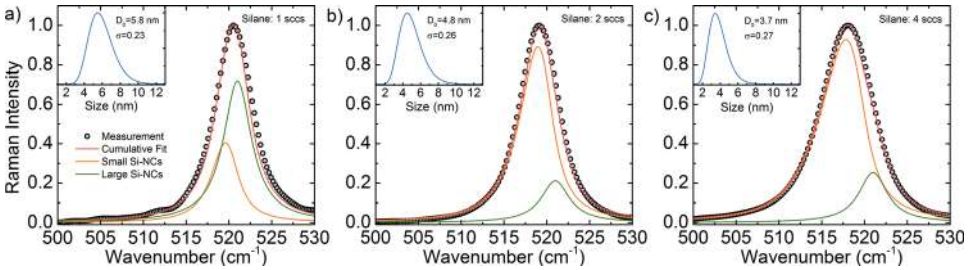

FIG. 6. Deconvoluted Raman spectrum of Si-NCs with a bimodal size distribution. Equations (11) and (13) are used for deconvolution of the data of large and small Si-NCs. Inset shows the size distribution of small Si-NCs, which is plotted after estimation of the parameters D_0 (mean size) and σ (skewness). Size distributions and skewness factors are determined with error values of about ± 0.1 nm, and about ~ 0.02, respectively.

Si-NCs do not demonstrate a shift in the Raman spectrum, the projection of the unshifted Lorentzian onto a size distribution function is unnecessary. We label the Raman spectrum of large Si-NCs as I_{large}. Second, we use the one-particle analytical PCM to represent small silicon nanocrystals and project it onto a size distribution function. In the present case[31] and in most of the other cases,[37–43] the particle size distribution is observed to be a lognormal distribution. Therefore, we use the lognormal function (Eq. (10)) in Eq. (12).

The next step is setting the integral boundaries within the frame of physical reasoning. According to the results, we demonstrate in Fig. 1, setting the largest size D_{max}, greater than 20 nm does not change the shape of the distribution for the particular case of silicon nanocrystals as larger sizes resemble bulk-like behavior (unshifted Lorentzian peak with no broadening). On the other hand, for most of the synthesis tools, the smallest Si-NCs that could be produced is about 1.0–2.0 nm as the smaller nanocrystals are considered as non-stable clusters.[44] Therefore, we set the integral boundaries from 2.0 nm to 20.0 nm. These integral boundaries are particular for the case of silicon nanocrystals and differ for other nanocrystal systems depending on the minimum stable size and on the degree of confinement. For small Si-NCs, we label the Raman spectrum as I_{small}. The experimental Raman spectrum of silicon nanocrystals with bimodal size distribution is therefore defined as

$$I_{\text{bimodal}} = \mathfrak{c}_{\text{small}} I_{\text{small}} + \mathfrak{c}_{\text{large}} I_{\text{large}}, \tag{14}$$

where $\mathfrak{c}_{\text{small}}$ and $\mathfrak{c}_{\text{large}}$ are the coefficients determined from the fitting procedure. Equation (14) has two physical parameters to be determined from the fitting of the experimental Raman spectrum of Si-NCs with bimodal size distribution: the mean size D_0 and the skewness σ, which are the essential parameters to determine the nanocrystal size distribution.

Figure 6 demonstrates the deconvoluted Raman spectra for various silane flow rates. By exploiting Eq. (14), we determine the mean sizes as 5.8, 4.8, and 3.7 nm (with error values of ± 0.1 nm); and skewness factors as 0.23, 0.26, and 0.27 (with error values of about ~ 0.02) for Si-NCs synthesized with silane flow rates of 1, 2, and 4 sccs, respectively. We insert the parameters in Eq. (13) to plot the size distribution of small Si-NCs. The result is shown in the insets of Fig. 6. We stress that the mean size of the particle size distribution differs from the peak position if the distribution is skewed. In a similar way, peak position of Raman spectrum for small Si-NCs differs from the position of the mean size and corresponds to the peak, or mode, of the particle size distribution. We estimate the modes of the size distributions as 5.5, 4.5, and 3.5 nm for the distributions demonstrated in Figs. 6(a)–6(c), respectively.

An important parameter on the analysis of synthesized nanocrystals with a multimodal size distribution is the volume fraction. From the deconvoluted Raman spectra, we can determine the volume fraction of small Si-NCs, η_{small}, in the analyzed volume. As a consequence of fact that the Raman scattering intensity is a volumetric information, we simply divide the integrated peak areas of small Si-NCs with the total integrated area of the small and large Si-NCs ($\eta_{\text{small}} = I_{\text{small}}/(I_{\text{small}} + I_{\text{large}})$). We determine the volume fraction of small Si-NCs roughly as 33%, 82%, and 84% for the Raman peaks demonstrated in Figs. 6(a)–6(c), respectively.

In order to benchmark the reliability of our results, we compare the peak sizes of small Si-NCs obtained from Raman spectroscopy to the sizes obtained from TEM and PL measurements. Figure 7 demonstrates the change in the peak size of small Si-NCs as a function of Raman shift estimated by employing Eq. (14). Each Raman measurement from a different sample (stars) is accompanied by its corresponding

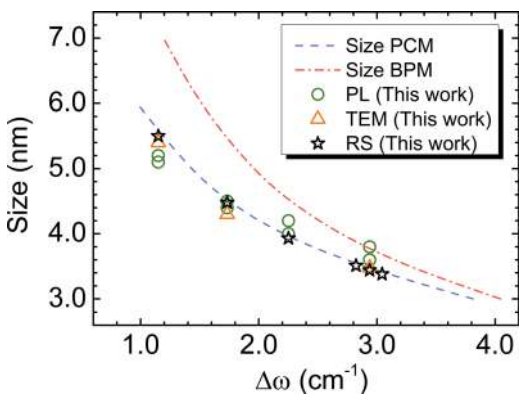

FIG. 7. Change in the peak size of small Si-NCs as a function of the absolute Raman peak shift to the lower wavenumbers with respect to the peak position of bulk c-Si (521 cm^{-1}) according to our approach based on the PCM. RS, PL, and TEM data are represented as stars, circles, and triangles, respectively. Each Raman measurement (stars) from a sample is accompanied by its corresponding PL and TEM data in the vertical direction. For comparison with PCM,[12] the BPM[21] is also demonstrated in the plot.

TEM (triangles) and PL (circles) data in the vertical direction. In addition to the experimental estimations, we demonstrate size dependent Raman shifts according to the PCM[12] and the BPM.[21] As evidenced from Fig. 7, peak sizes of small Si-NCs obtained from TEM and PL are within close proximity of the sizes obtained from RS. In addition, exploiting our analytical PCM produces similar results to the PCM, which is also demonstrated in Fig. 3. As the experimental data from TEM and PL follow the PCM trend, we conclude that using PCM-based approach for size determination yields more realistic results with respect to the BPM.

The analytical formulation of the PCM, which we introduce in this work, enables accurate determination of the size distribution of confined silicon nanocrystals, even in the case of a multimodal distribution. In addition, it agrees well with the PCM in the case of size distributions, even though the smallest sizes are involved. This is due to the fact that the smallest sizes usually occupy the tail of a size distribution. Using symmetric Lorentzian function preserves the shape of the size distribution, but probably leads to a deviation in the low end tail of the distribution. In the case of monodisperse sizes, Eq. (10) could still be used for determination of the nanocrystal size from the experimental Raman spectrum. However, as the peak shape becomes more asymmetric for sizes smaller than 2.0 nm, use of Eq. (10) could result in deviation of the determined size with respect to the actual nanocrystal size. In this case, we suggest to use Eq. (8) for size determination. In most cases, 2.0 nm is the critical limit for a silicon cluster to be considered as a stable nanocrystal—especially for the gas phase synthesis methods[11,44–47] —and synthesis of silicon nanocrystals (either monodisperse or dispersed) smaller than 2.0 nm is unlikely. For this reason, exploiting Eq. (10) to analyze Si-NCs with small sizes and monodisperse distributions produces correct results. On the other hand, using the set of formulations in Eq. (11) is sufficient for estimation of the nanocrystal size if the distribution is monodisperse.

Equation (12) is a rigorous formulation as it consists of two separately usable parts: an analytical, non-integral Lorentzian definition of Raman intensity; and a distribution function, which needs to be integrated over the size. The flexibility of exploiting Eq. (12) is the freedom of selecting any type of distribution function in the integral—depending on the nanocrystal size distribution, e.g., lognormal, normal, or logistic distribution—by keeping the one-particle analytical PCM unaffected from the integration. The method we use here could be applied to other nanocrystal systems, such as Ge,[27] SnO_2,[48] TiO_2,[49] and diamond.[50] The task one should achieve is the re-formulation of Eq. (11) for the particular nanocrystal system to be analyzed.

Figure 7 concludes that Raman spectroscopy can be preferred for the size estimation of Si-NCs instead of photoluminescence spectroscopy and transmission electron microscopy. When compared with these techniques, Raman spectroscopy does not require sample preparation and provides the information in a time-efficient manner. These features provide rapid feedback to the synthesis technique about the size distribution. This advantage possibly enables better optimization of the process parameters to achieve the absolute control on the size and size distribution.

V. CONCLUSION

In conclusion, we use Raman spectroscopy for the direct analysis of the size distribution and volume fraction of silicon nanocrystals (Si-NCs). These analyses are performed deconvoluting the experimental Raman spectra by using a rigorously derived one-particle analytical approach based on the phonon confinement model. Estimated peak sizes of small Si-NCs are in close agreement with the sizes obtained from transmission electron microscopy and photoluminescence spectroscopy. These results demonstrate that Raman spectroscopy can potentially be a standard diagnostic tool for the accurate size analysis of confined nanocrystals with free-standing morphology. Moreover, as a fast and simple analysis technique, Raman spectroscopy can potentially enable rapid process optimization route during nanomaterials synthesis, which is a critical requirement for reaching optimum size control for any synthesis tool.

ACKNOWLEDGMENTS

This work was part of the research programme of the Foundation for Fundamental Research on Matter (FOM), which is part of the Netherlands Organisation for Scientific Research (NWO). Authors of this work thank M. J. F. van de Sande for skillful technical assistance, M. A. Verheijen for TEM images, and the group of Tom Gregorkiewicz for PL measurements.

[1]L. Hu, H. Wu, S. Hong, L. Cui, J. McDonough, S. Bohy, and Y. Cui, Chem. Commun. **47**, 367 (2011).
[2]A. Dâna, İ. Akça, O. Ergun, A. Aydınlı, R. Turan, and T. G. Finstad, Phys. E: Low-Dimens. Syst. Nanostruct. **38**, 94 (2007).
[3]J. De La Torre, A. Souifi, A. Poncet, C. Busseret, M. Lemiti, G. Bremond, G. Guillot, O. Gonzalez, B. Garrido, J. R. Morante, and C. Bonafos, Phys. E: Low-Dimens. Syst. Nanostruct. **16**, 326 (2003).
[4]G. Conibeer, M. Green, R. Corkish, Y. Cho, E.-C. Cho, C.-W. Jiang, T. Fangsuwannarak, E. Pink, Y. Huang, T. Puzzer, T. Trupke, B. Richards, A. Shalav, and K. Lin, Thin Solid Films **511–512**, 654 (2006).
[5]C. Sevik and C. Bulutay, Phys. Rev. B **77**, 125414 (2008).
[6]M. Govoni, I. Marri, and S. Ossicini, Nat. Photonics **6**, 672 (2012).
[7]D. Timmerman, J. Valenta, K. Dohnalová, W. D. A. M. De Boer, and T. Gregorkiewicz, Nat. Nanotechnol. **6**, 710 (2011).
[8]S. Huang and G. Conibeer, J. Phys. D: Appl. Phys. **46**, 024003 (2013).
[9]D. Comedi, O. Zalloum, E. Irving, J. Wojcik, T. Roschuk, M. Flynn, and P. Mascher, J. Appl. Phys. **99**, 023518 (2006).
[10]H. Borchert, E. Shevehenko, A. Robert, I. Mekis, A. Kornowski, G. Grubel, and H. Weller, Langmuir **21**, 1931 (2005).
[11]G. Ledoux, J. Gong, F. Huisken, O. Guillois, and C. Reynaud, Appl. Phys. Lett. **80**, 4834 (2002).
[12]G. Faraci, S. Gibilisco, P. Russo, A. R. Pennisi, and S. La Rosa, Phys. Rev. B **73**, 033307 (2006).
[13]V. Paillard, P. Puech, M. A. Laguna, R. Carles, B. Kohn, and F. Huisken, J. Appl. Phys. **86**, 1921 (1999).
[14]S. Godefroo, M. Hayne, M. Jivanescu, A. Stesmans, M. Zacharias, O. I. Lebedev, G. Van Tendeloo, and V. V. Moshchalkov, Nat. Nanotechnol. **3**, 174 (2008).
[15]G. Gouadec and P. Colomban, Prog. Cryst. Growth Charact. Mater. **53**, 1 (2007).
[16]C. Smit, R. A. C. M. M. Van Swaaij, H. Donker, A. M. H. N. Petit, W. M. M. Kessels, and M. C. M. Van de Sanden, J. Appl. Phys. **94**, 3582 (2003).
[17]W. Ke, X. Feng, and Y. Huang, J. Appl. Phys. **109**, 083526 (2011).
[18]C. M. Hessel, J. Wei, D. Reid, H. Fujii, M. C. Downer, and B. A. Korgel, J. Phys. Chem. Lett. **3**, 1089 (2012).
[19]S. Muthmann, F. Köhler, M. Meier, M. Hülsbeck, R. Carius, and A. Gordijn, J. Non-Crystall. Solids **358**, 1970 (2012).
[20]H. Richter, Z. P. Wang, and L. Ley, Solid State Commun. **39**, 625 (1981).

[21]J. Zi, H. Buscher, C. Falter, W. Ludwig, K. Zhang, and X. Xie, Appl. Phys. Lett. **69**, 200 (1996).
[22]S. K. Gupta and P. K. Jha, Solid State Commun. **149**, 1989 (2009).
[23]D. Barba, F. Martin, and G. G. Ross, Nanotechnology **19**, 115707 (2008).
[24]R. Tubino, G. Zerbi, and L. Piseri, J. Chem. Phys. **56**, 1022 (1972).
[25]T. R. Hart, R. L. Aggarwal, and B. Lax, Phys. Rev. B **1**, 638 (1970).
[26]I. H. Campbell and P. M. Fauchet, Solid State Commun. **58**, 739 (1986).
[27]K. Roodenko, I. A. Goldthorpe, P. C. McIntyre, and Y. J. Chabal, Phys. Rev. B **82**, 115210 (2010).
[28]A. C. A. Silva, E. S. F. Neto, S. W. da Silva, P. C. Morais, and N. O. Dantas, J. Phys. Chem. C **117**, 1904 (2013).
[29]M. Grimsditch and M. Cardona, Phys. Status Solidi B **102**, 155 (1980).
[30]J. Zi, K. Zhang, and X. Xie, Phys. Rev. B **55**, 9263 (1997).
[31]İ. Doğan, N. J. Kramer, R. H. J. Westermann, K. Dohnalova, A. H. M. Smets, M. A. Verheijen, T. Gregorkiewicz, and M. C. M. van de Sanden, J. Appl. Phys. **113**, 134306 (2013).
[32]G. Faraci, S. Gibilisco, and A. R. Pennisi, Phys. Rev. B **80**, 193410 (2009).
[33]R. Gupta, Q. Xiong, C. K. Adu, U. J. Kim, and P. C. Eklund, Nano Lett. **3**, 627 (2003).
[34]C. Delerue, G. Allan, and M. Lannoo, Phys. Rev. B **48**, 11024 (1993).
[35]S. Manotas, F. Agulló-Rueda, J. D. Moreno, F. Ben-Hander, and J. M. Martínez-Duart, Thin Solid Films **401**, 306 (2001).
[36]A. L. Patterson, Phys. Rev. **56**, 978 (1939).
[37]R. E. De Lamaestre and H. Bernas, Phys. Rev. B **73**, 125317 (2006).
[38]J. Söderlund, L. B. Kiss, G. A. Niklasson, and C. G. Granqvist, Phys. Rev. Lett. **80**, 2386 (1998).
[39]C. G. Granqvist and R. A. Buhrman, J. Appl. Phys. **47**, 2200 (1976).
[40]A. Gupta and H. Wiggers, Nanotechnology **22**, 055707 (2011).
[41]X. J. Hu, Y. H. Lu, and Y. G. Shen, Solid State Commun. **149**, 903 (2009).
[42]N. Saxena, P. Kumar, D. Kabiraj, and D. Kanjilal, Nanoscale Res. Lett. **7**, 547 (2012).
[43]S. Alkis, A. K. Okyay, and B. Ortaç, J. Phys. Chem. C **116**, 3432 (2012).
[44]L. Boufendi, M. C. Jouanny, E. Kovacevic, J. Berndt, and M. Mikikian, J. Phys. D: Appl. Phys. **44**, 174035 (2011).
[45]N. Rao, S. Girshick, J. Heberlein, P. McMurry, S. Jones, D. Hansen, and B. Micheel, Plasma Chem. Plasma Process. **15**, 581 (1995).
[46]L. Mangolini, E. Thimsen, and U. Kortshagen, Nano Lett. **5**, 655 (2005).
[47]R. Gresback, T. Nozaki, and K. Okazaki, Nanotechnology **22**, 305605 (2011).
[48]A. Diéguez, A. Romano-Rodríguez, A. Vilá, and J. R. Morante, J. Appl. Phys. **90**, 1550 (2001).
[49]D. Bersani, P. P. Lottici, and X.-Z. Ding, Appl. Phys. Lett. **72**, 73 (1998).
[50]M. Lipp, V. Baonza, W. Evans, and H. Lorenzana, Phys. Rev. B **56**, 5978 (1997).